POLITECNICO DI TORINO
Repository ISTITUZIONALE

Adaptable Meta-Signal Tracking for Next-Generation Satellite Navigation Systems and LEO PNT

Original
Adaptable Meta-Signal Tracking for Next-Generation Satellite Navigation Systems and LEO PNT / Nardin, A., Dovis, F., Zanier, F., Melman, F.. - In: IEEE ACCESS. - ISSN 2169-3536. - 13:(2025), pp. 5706-5718. [10.1109/access.2025.3526334]

Availability:
This version is available at: 11583/2996510 since: 2025-01-10T17:37:42Z

Publisher:
IEEE

Published
DOI:10.1109/access.2025.3526334

Terms of use:

This article is made available under terms and conditions as specified in the corresponding bibliographic description in the repository

Publisher copyright

(Article begins on next page)

18 November 2026

IEEE Access
Multidisciplinary | Rapid Review | Open Access Journal

Received 4 December 2024, accepted 31 December 2024, date of publication 6 January 2025, date of current version 10 January 2025.

Digital Object Identifier 10.1109/ACCESS.2025.3526334

RESEARCH ARTICLE

Adaptable Meta-Signal Tracking for Next-Generation Satellite Navigation Systems and LEO PNT

ANDREA NARDIN[1], (Member, IEEE), FABIO DOVIS[1], (Member, IEEE), FRANCESCA ZANIER[2], AND FLOOR MELMAN[2]

[1]Department of Electronics and Telecommunications, Politecnico di Torino, 10124 Turin, Italy
[2]European Space Agency, AZ 2201 Noordwijk, The Netherlands

Corresponding author: Andrea Nardin (andrea.nardin@polito.it)

This work has been developed in the framework of the activity INNovative User receiver processing and ENhanced signals in gnss DOmain (INNUENDO) funded by the European Space Agency (ESA). The project was carried out in the scope of investigating "Enhanced GNSS signals in space and user receiver processing" in response to ESA AO-1-9585/19/NL/CRS, Activity No. 1000023741 in the "esa-star" system, Item no. 18.1ET.29.

ABSTRACT In this study, the concept of multichannel signal tracking, previously discussed in the Global Navigation Satellite System literature, is expanded towards next-generation satellite navigation paradigms by leveraging multiple narrowband signals that are synchronously transmitted from the same satellite. This approach achieves a performance comparable to that of signals transmitted over larger bandwidths while effectively reallocating frequency resources to enhance the capacity of a wideband communication channel. This methodology can be applied to orthogonal signals, independently from their respective modulations and regardless of whether they are transmitted over different carrier frequencies or occupy the same bandwidth. The resulting architecture is tested in modern positioning, navigation and timing (PNT) scenarios, addressing in particular, the forthcoming low earth orbit (LEO) PNT paradigm to broad the technique's applicability also towards potential piggybacked services hosted by broadband megaconstellations (e.g. Kuiper, Starlink). The applicability domain of the signal tracking architecture is explored through a parametric analysis, assessing the performance under different combined conditions such as transmission bands, multichannel combination modes, Doppler profiles, and propagation conditions. This technique has shown large performance improvements with respect to conventional single channel processing, yielding code estimation error reductions above 90% in almost all the tested conditions.

INDEX TERMS Global navigation satellite systems, multichannel, meta-signal, signal tracking, LEO PNT, megaconstellation, satellite navigation, satellite broadcast, Kuiper, starlink.

I. INTRODUCTION

Positioning, navigation, and timing (PNT) services are at the core of many applications [1]. Besides earth-based navigation, also vehicle and inter-personal ranging [2], [3], [4], broadband communication networks [5], precision agriculture [6], or space applications [7], [8], [9], [10], are among the relevant domains. In recent years, ensuring accurate PNT services has become increasingly challenging, especially considering the diverse range of applications involved. However, the growing number of existing and anticipated applications necessitates a PNT system that is both precise and reliable [1], [11], [12], even under challenging Doppler conditions, which are further intensified in vehicular applications. In the field of Global Navigation Satellite Systems (GNSSs), researchers and experts have introduced various approaches to meet these demands. These approaches include advancements in signal design and modulations [13], [14], [15], [16] as well as innovative signal processing architectures [17], [18], [19].

The associate editor coordinating the review of this manuscript and approving it for publication was Zheng H. Zhu.

© 2025 The Authors. This work is licensed under a Creative Commons Attribution 4.0 License.
For more information, see https://creativecommons.org/licenses/by/4.0/

In parallel, a diversified offer of PNT services is growing [1], enabled by the simultaneous broadcasting of multiple signals [20]. In the context of a satellite constellation providing multiple PNT services, it is indeed possible for each satellite payload to transmit more than one direct sequence spread spectrum (DSSS) signal component, often called *channels* in the GNSS domain [21]. These components are typically synchronized and maintain a certain degree of coherence, particularly when they are multiplexed in a single composite signal and undergo the same transmission chain, including frequency up-conversion, amplification, and antenna processes [15], [22], [23]. While multiple channel availability is already established in GNSSs [20], it is also expected that future advancements in alternative and complementary PNT technologies, will likely incorporate some form of service multiplicity [24], [25], [26], [27], [28], [29], [30].

The availability of synchronous channels can be exploited to improve the data demodulation and increase the precision of the position estimate through a *multichannel* approach and, although not foreseen by the service provider, it can be implemented within the signal processing chain of a receiver. Intuitively, these signals embed the same range information and such coherency can be exploited to improve the quality of the estimation.

In recent studies, researchers have explored the concept of a *meta-signal*, which refers to a unified signal composed of synchronous GNSS channels received at different frequencies [31], [32], [33], [34]. The utilization of meta-signals as a single wideband signal has emerged as a promising technique for leveraging multiple channel resources and obtaining precise measurements to enhance positioning accuracy and data demodulation [33], [34], [35], [36], [37], [38]. Additionally, this approach offers improved resilience against common issues like multipath and interference [39]. In the context of a traditional receiver architecture for GNSS, the coherent processing of multiple signals occurs at the tracking stage [40]. This integration takes place early in the signal processing chain and aims to maximize the accuracy of measurements by combining the information content from different signals [22], [23], [39], [41], [42], [43].

One notable challenge associated with meta-signals, which affects also split-spectrum modulations, is the presence of a multi-peaked autocorrelation function (ACF) [44]. This characteristic can introduce biases in measurements and false locking, requiring careful consideration in practical implementations. Additionally, the conventional approach to constructing meta-signals is limited to jointly processing signal components transmitted over different carrier frequencies, while modern GNSSs often transmit signal components within the same bandwidth using in-phase and quadrature carriers (e.g., Galileo E5a-I and E5a-Q) or orthogonal pseudo-random codes (e.g., E1B and E1C) [45]. This approach may not align with the future requirements of emerging PNT technologies and GNSSs.

For instance, in low earth orbit (LEO) PNT systems [16], [25], [46], payload designs typically prioritize rapid reconfiguration and efficient resource utilization, and might adopt signal components that share the same bandwidth [47]. This would be especially true for piggybacked PNT services hosted on broadband *megaconstellations*, such as Amazon's Kuiper or SpaceX's Starlink [26], [48], [49], [50], [51], where restricting a secondary PNT service to narrowband channels would be preferred. Furthermore, when LEO satellite signals are received by Earth-based terminals, they undergo substantial Doppler shifts [52], exacerbated in vehicular applications, and resulting in significant distortion, particularly for wideband signals.

In order to overcome these limitations, we proposed a generalized approach to meta-signal construction that encompasses the combination of signal components transmitted within the same bandwidth [28], [29], [53]. This expansion of the multichannel approach allows for the incorporation of various forms of signal orthogonality beyond frequency separation. This flexible approach can be adapted to different signal configurations and the specific requirements of diverse payloads. Furthermore, it promotes efficient bandwidth utilization by enabling the use of narrower signal bandwidths, leading to enhanced resilience against challenging Doppler effects [28] and allowing an adaptable accommodation of communication channels.

A previous exploration of this concept, referred to as *virtual wideband (VWB) tracking*, has been conducted in specific case studies [28], [54]. Nonetheless, a comprehensive analysis of its performance under demanding scenarios has yet to be addressed, and its applicability range requires careful investigation. It is crucial to assess the robustness of the method to different implementation conditions, especially under possible bandwidth limitations and harsh environments that may characterize modern GNSS scenarios and integrated navigation and communication systems [55]. These conditions include high frequencies, narrow signal bandwidths, significant Doppler effects, and multipath interference.

In this work we characterize this flexible meta-signal tracking architecture, along with its applicability, in the challenging context of LEO PNT and megaconstellations. This involves a comprehensive understanding of the PNT system's capabilities and limitations within this specific domain. We evaluate the performance of the proposed method in different demanding LEO PNT scenarios, where the signal tracking response to challenging conditions is thoroughly examined and compared against a benchmarking single channel (SC) architecture. In particular, a parametric analysis is carried out to investigate the applicability domain of the proposed technique under different working scenarios with respect to the transmission band, the multichannel combination strategy, the Doppler profile, and the propagation conditions (i.e. line of sight (LOS), multipath).

The rest of the article is structured as follows. In Section II, the rationale behind meta-signals is discussed, together with

the conventional approach commonly used. We then provide a detailed description of the proposed implementation and highlight any potential concerns or limitations. The methodology that drove the testing campaign is described in Section III, while the results are discussed in Section IV. Conclusions are drawn in Section V.

II. A MULTICHANNEL TRACKING ARCHITECTURE

A. THE META-SIGNAL RATIONALE

The well-known Cramér-Rao bound (CRB) sets a lower limit on the variance σ_τ^2 of a propagation time estimator for time of arrival (TOA) estimation [56]. Such a limit can be expressed as:

$$\sigma_\tau^2 \geq \frac{1}{8\pi^2\eta\beta^2} = \frac{1}{8\pi^2\frac{C}{N_0}T\beta^2}. \tag{1}$$

Here, β^2 represents the square of the Gabor bandwidth, which is defined as:

$$\beta^2 \triangleq \frac{\int_{-\infty}^{+\infty} f^2|X(f)|^2}{\int_{-\infty}^{+\infty}|X(f))|^2}. \tag{2}$$

The Gabor bandwidth is dependent on the spectrum $X(f)$, which is the Fourier transform of the noiseless observed baseband signal $x(t)$ [56], [57]. Notably, equation (1) emphasizes the dependence on the signal-to-noise ratio (SNR), denoted as $\eta = \frac{C}{N_0}T$ [44], [57], where T represents the observation time and $\frac{C}{N_0}$ is the *carrier-to-noise-density ratio* (C/N_0).

By increasing the Gabor bandwidth as indicated in (1), it becomes possible to decrease the CRB for the propagation time estimator. This, in turn, leads to improved position estimation in those radio navigation systems that rely on TOA measurements. Over the years, various solutions have been proposed in the GNSS literature to achieve a larger Gabor bandwidth. These solutions primarily differ in how they obtain a spectrum $X(f)$ with a wide Gabor bandwidth.

Traditionally, a straightforward and widely-known approach involves using single signals with a wide bandwidth. However, in recent years, a novel approach has emerged, which involves jointly processing multiple signals received over different carrier frequencies to achieve enhanced resolution. This approach is commonly known as the utilization of GNSS *meta-signals* [36].

B. A GENERALIZED APPROACH TO META-SIGNALS

Consider a signal $x(t)$ being processed by a TOA estimator. According to (1), it is desirable for $x(t)$ to possess a wide Gabor bandwidth. Now, let's examine a set of N signals $s_i(t)$ with $i = 1, \ldots, N$. Under a multichannel approach, a large Gabor bandwidth can be achieved if the processed channel components are distributed across the spectrum of $x(t)$ in such a way that

$$x(t) = \sum_{i=1}^{N} s_i(t)e^{j2\pi f_i t}. \tag{3}$$

This ensures that a significant portion of the energy of $x(t)$ is located at the edges of its spectrum. An approximation of (3) can be easily obtained by considering a complex baseband of a received Radio Frequency (RF) signal if the relative frequency separation between the signal components—given by f_i—within $x(t)$ matches the frequency separation among the components in the transmitted RF signal. This composite signal, consisting of multiple channels and processed as a single signal, is referred to as a *meta-signal* (in this case, generalized to N signals).

However, if each signal $s_i(t)$ can be individually processed by a receiver, it is possible to effectively obtain a composite signal within the receiver's processing chain. Indeed, a signal whose complex baseband has the form in (3) can be achieved by modulating each carrier at frequency f_i with the i-th signal component $s_i(t)$. The resulting composite signal still exhibits a wide Gabor bandwidth and can be utilized by a TOA estimator. It is important to highlight that this approach relies on the assumption that signal components can be processed independently, essentially meaning they are orthogonal to each other. Consequently, this generalized meta-signal construction can also be extended to components transmitted over the same bandwidth, such as through the use of in-phase and quadrature carriers or orthogonal spreading codes.

Correlators are commonly employed in the implementation of TOA estimators. The correlation properties of a signal $x(t)$ can be accurately described by its ACF, given by

$$R_{xx}(\tau) = \int_{-\infty}^{+\infty} x(t+\tau)x^*(t)\,\mathrm{d}t. \tag{4}$$

A signal with a wide Gabor bandwidth exhibits a narrow main peak in its ACF. This characteristic is closely associated with improved code-tracking performance, indicating precise TOA estimation [58]. However, it can be shown [59]that the ACF of a meta-signal, as defined in (3), is equivalent to the sum of the ACFs of its component signals modulating complex exponentials, if frequency-shifted components $s_i(t)$ are confined to disjoints bandwidths. In other words, it can be expressed as

$$R_{xx}(\tau) = \sum_{i=1}^{N} R_{x_i x_i}(\tau) = \sum_{i=1}^{N} R_{s_i s_i}(\tau)e^{j2\pi f_i \tau} \tag{5}$$

where $x_i(t) = s_i(t)e^{j2\pi f_i t}$.

As an example, consider two BPSK(1) signals, $s_1(t)$ and $s_2(t)$, with carrier frequencies separated by f_m. In this scenario, a meta-signal can be defined as follows:

$$x(t) = s_1(t)e^{-j2\pi\frac{f_\mathrm{m}}{2}t} + s_2(t)e^{+j2\pi\frac{f_\mathrm{m}}{2}t}. \tag{6}$$

The power spectral density (PSD) corresponding to this meta-signal is illustrated in Fig. 1. As observed from the figure, this multichannel signal possesses a wide Gabor bandwidth, as defined in (2). It can be demonstrated that this property results in a sharp ACF, which has been shown to enhance code delay estimation [58], [60]. Fig. 2 depicts the

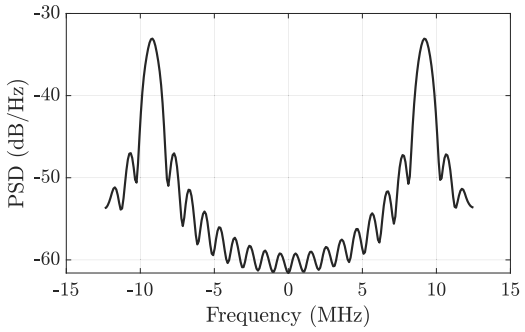


FIGURE 1. PSD example of a BPSK(1) and a BPSK(1) signal, separated by 18.414 MHz.

ACF of the signal in this example, comparing the ACFs of the individual component signals with the meta-signal.

It is important to note that meta-signals often face a significant challenge in the form of a multi-peaked ACF, as also highlighted in Fig. 2. At low SNR, the presence of noise in the signal can cause side peaks to surpass the main peak. In a typical correlator, this could lead to false locking on a correlation peak that is not the main one, resulting in biased TOA estimation. This issue is well-known for narrowband signals and Binary Offset Carrier (BOC) modulations [61], [62]. For meta-signals, the number of peaks and, thus, the severity of this ambiguity depend on the frequency separation between the combined channels. Therefore, an effective implementation of meta-signal tracking must overcome this downside. Nonetheless, it is possible to leverage the interconnected characteristics of a meta-signal to achieve improved TOA estimation, regardless of how the signal $x(t)$ is obtained.

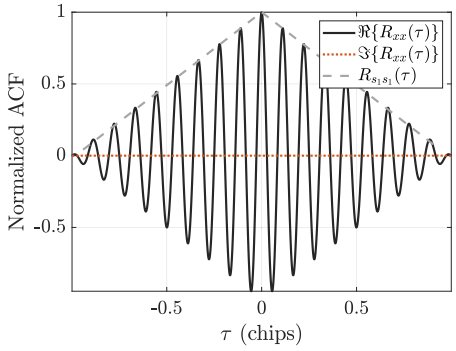


FIGURE 2. ACF of a single BPSK(1) signal and a meta-signal made by two BPSK(1) channels with a 18.414 MHz separation.

C. A VIRTUAL WIDEBAND ARCHITECTURE

Taking into account the aforementioned factors, a signal tracking architecture for multiple channels has been created to efficiently handle a meta-signal characterized by a complex baseband representation described in equation (3). By extending the concept of meta-signal to encompass any form of signal orthogonality, this architecture is capable of independently processing narrowband signal components and generating individual carrier signals at f_i for achieving a VWB meta-signal. The VWB signal is virtually obtained during the post-correlation stage, capitalizing on the property expressed in (5).

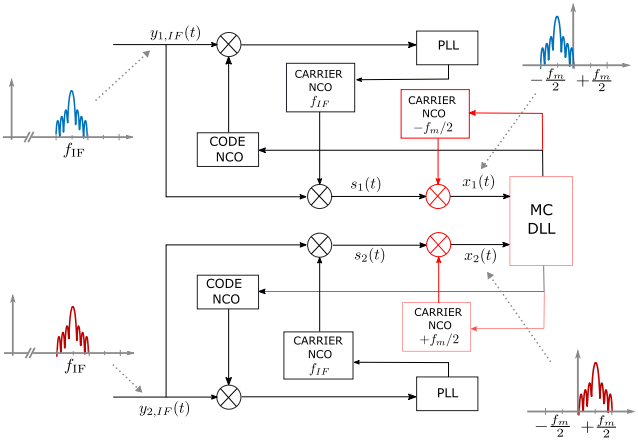


FIGURE 3. Virtual Wideband tracking implementation (second step). Distinctive blocks highlighted in red.

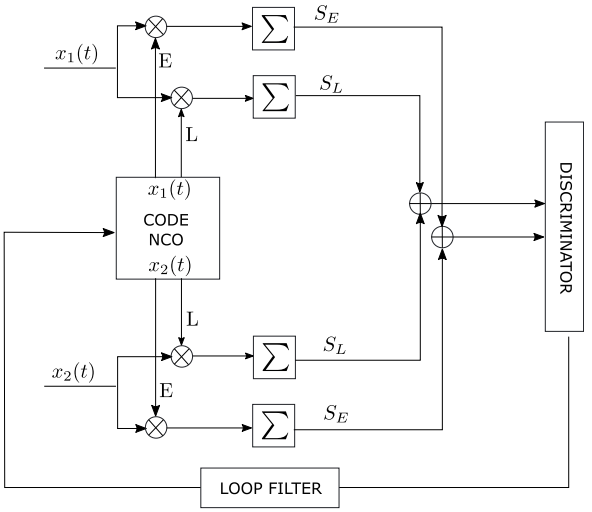


FIGURE 4. Multichannel (MC) delay-locked loop (DLL) implementation. From [54].

The architectural arrangement depicted in Fig. 3 demonstrates the implementation of the VWB concept in a closed-loop manner. This arrangement describes, without loss of generalization, a tracking stage with $N = 2$ channels. Two received signals undergo frequency down-conversion to intermediate frequency (IF) (or baseband) before being directed to the signal tracking stage of a receiver ($y_{1,\mathrm{IF}}(t)$ and $y_{2,\mathrm{IF}}(t)$). Following this, they pass through two interrelated loops for carrier and code wipe-off, which are typical of a GNSS receiver's tracking stage [20]. Prior to entering a multichannel DLL, as a preliminary conditioning operation, the signals are mixed with a local carrier. This carrier is generated by a numerically-controlled oscillator (NCO)

driven by the DLL, and it enables the desired frequency separation f_{m} between the processed components. Descriptive representations of the one-sided signal spectra are included in Fig. 3 to illustrate how the spectral characteristics evolve throughout the processing chain.

The two channels are integrated within the DLL, at the post-correlation level (as shown in Fig. 4). This approach is deemed appropriate due to the property described in (5), which states that the ACF of a meta-signal equals the sum of side-band ACFs of each channel, therefore enabling the combination of each channel's correlator output rather than merging the components to build the meta-signal $x(t)$ prior to correlation. The proposed scheme employs a conventional *early-late* (E-L) architecture for this purpose.

To overcome the issue of peak ambiguity, it is necessary for a functional tracking stage implementation to employ suitable techniques, such as methods developed for high-order BOC modulations [63], [64]. [59]. For a non-exhaustive discussion on ambiguity resolution methods for meta-signals, please refer to [59]. Another method, enabled by the inherent flexibility of meta-signals and adopted in this work, entails implementing a *two-step* processing of the composite signal. In the initial step, each signal component is independently tracked—through a standard SC architecture [40]—and characterized by an unambiguous ACF such as the one indicated by the gray dashed line in Fig. 2. This allows the correlators to align unambiguously with the main peak of the solid black line as well [32]. This method enables a seamless transition from a SC step, where a conventional tracking stage is used, to a MC step when adopting the architecture depicted in Fig. 3. Following the initial SC tracking, the MC processing is initiated based on a locking condition, which could be determined using a phase lock indicator (PLI) [28], [65]. The MC stage is activated once the PLI surpasses a predefined threshold, which is defined as a receiver parameter. In this phase a sharper ACF allows to tolerate stronger noise and therefore bearing a reduced E-L correlators spacing, which enables a more accurate signal tracking. An equivalent gain yielded by the same E-L spacing reduction applied to plain SC processing could not have been attained due to the smaller (and less robust) gap between early or late and prompt correlator outputs in tracking lock conditions.

Fig. 5 offers an overview of the sequential stages involved in the process. It is important to note the utilization of a σ-*aware channel selector* choosing among the N SC tracking output streams to initialize the MC code NCO and DLL loop filter blocks. The selection process relies on the statistical characteristics of the filtered discriminator output, as estimated by each SC tracking stage. Specifically, it selects the channel with the least discriminator output variance, estimated over an observation time window, to initialize the subsequent MC stage and therefore ensuring a more resilient transition between the SC and MC steps. The introduction of the selector leverages signal diversity by prioritizing the channel that likely ensures the more robust multichannel processing.

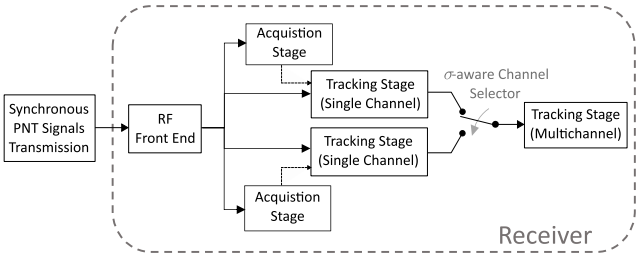


FIGURE 5. Receiver stages and decision logic using a two-step ambiguity resolution method. Example with $N = 2$ channels. From [54].

III. METHODOLOGY

A. STUDY LOGIC

An evaluation of performance was conducted addressing modern GNSSs and specifically for LEO PNT scenarios. A parametric analysis was setup to study the architecture response to different transmission bands, Doppler and received signal power characteristics, type of combined channels, and propagation conditions (i.e. LOS or multipath (MP)). The varying scenario paramaters under test are summarized in Table 1.

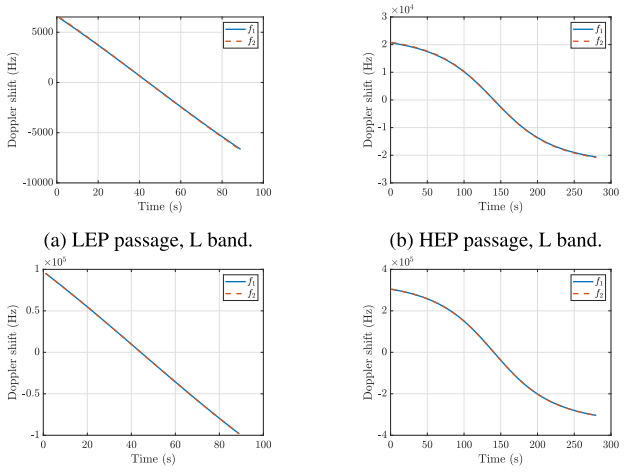
TABLE 1. Parameters under test.

Parameter under test	Range of variation
Freq. bands	• L band (central frequency f_c= 1062 MHz) • K_u band (central frequency f_c= 15665 MHz)
Doppler conditions	• low elevation peak (LEP) satellite passage • high elevation peak (HEP) satellite passage
Meta-signal components	• Configuration S1: two BPSK(1) channels transmitted at the same carrier frequency f_1=f_c • Configuration S2: two BPSK(1) channels transmitted at two carrier frequencies, f_1=f_c and f_2=f_1 + 10 MHz
LOS conditions	• two-ray MP propagation: Signal-to-multipath ratio (SMR) = 6 dB; reflected signal (RS) delay = 0.5 chips • LOS propagation

The analysis is focused on two frequency bands in the L and K_u bands. They were chosen with the intent of spanning a wide range of use-cases frequencies, from the L-band (e.g. GNSSs), to the K_u band (e.g. Amazon's upcoming megaconstellation Kuiper [66]). They allow, in fact, to (*i*) assess the performance under low and high Doppler shift levels (K_u band signals experience an about 15 times stronger Doppler shift); and (*ii*) to test signals with different average C/N_0 (around 25 dB of difference between L and K_u band). Higher bands such as the K_a band have been left out from the available choices because they experience an intense Doppler effect, that causes Doppler frequency shifts that are at least 30 times larger than signals in the L band. Moreover, signals in the K_a band are subject to a strong atmospheric absorption

that greatly reduces the received signal power. These aspects contribute to the impossibility to successfully track signals in the K_a band, transmitted under the current configurations.

To introduce diversity in the Doppler scenarios, two distinct satellite passages were examined. A LEP passage represented mild Doppler conditions characterized by a predominantly linear profile and a relatively low average C/N_0. Conversely, a HEP passage, simulated intense Doppler conditions. This passage occurred above the zenith and exhibited a generally non-linear Doppler profile accompanied by a higher average C/N_0. The specific characteristics of these trajectories are contingent upon the configuration of the satellite constellation. Consequently, distinct Doppler profiles were computed for each carrier frequency. Each test was repeated for both LEP and HEP satellite passage profiles. Fig. 6 illustrates the Doppler shift of the two different satellite passages, for each frequency band.



(a) LEP passage, L band. (b) HEP passage, L band.

(c) LEP passage, K_u band. (d) HEP passage, K_u band.

FIGURE 6. Doppler shift for different satellite passages, frequency carriers, and combined signal configurations (S1 and S2).

By means of these parametrical tests, we compared the performance of two different types of signal combinations, possible thanks to the flexibility of the generalized meta-signal approach. A signal configuration, namely *S1*, allows to jointly process two signals transmitted over the same bandwidth, thus fostering an efficient use of the transmission bandwidth. Conversely, in the *S2* signal configuration we process a meta-signal made by two signals, that are transmitted over adjacent frequency bands, whose carrier frequency separation is defined in Table 1. The two different signal configurations S1 and S2 were defined to target different challenges. Signal S1 is efficient in terms of transmission bandwidth resources and its two component channels are subject to the same Doppler shift. On the contrary, the component channels of signal S2 experience a slightly different Doppler shift, making the signal configuration more challenging to track for the VWB architecture, especially under intense Doppler effect and strong signal attenuation (i.e. in the K_u band). Notice that for both configurations the resulting virtual frequency separation injected in the receiver processing architecture will be the same to ensure a fair comparison.

Each test is also repeated twice: using LOS signals and using two-ray MP signals. The two-ray model uniquely introduces the risk of false locks—a critical condition for testing robustness in meta-signal processing. In contrast, more realistic multipath models, while better representing actual environments, typically do not induce such harmful effects, as a result of the rapid geometry changes relative to the bandwidth of the DLL [67]. These effects are characteristic of LEO satellites; however, they are largely determined by design parameters such as carrier frequency and orbital height [47], [67]. The two-ray model, therefore, serves as an essential tool for evaluating worst-case scenarios while ensuring general applicability by remaining independent of specific constellation design assumptions. Additionally, it enables an isolated analysis of primary multipath effects, improving explainability while reducing computational complexity. This approach aligns with the parametric analysis goals of this work, ultimately providing a challenging yet controlled scenario for performance evaluation.

Table 1 lists the scenario parameters that are varying throughout the tests. The combination of this parameters arrangements produces 16 signals generation scenarios, which are addressed in 8 different tests, each comparing S1 and S2 signals, which are listed in Table 2 alongside their test IDs.

TABLE 2. Test-dependent conditions.

Doppler conditions	Test ID	Freq. band	Satellite passage	Visibility
Mild	LS1	L	LEP	LOS
	MP1	L	LEP	two-ray MP
Moderate	LS2	L	HEP	LOS
	MP2	L	HEP	two-ray MP
	LS3	K_u	LEP	LOS
	MP3	K_u	LEP	two-ray MP
Severe	LS4	K_u	HEP	LOS
	MP4	K_u	HEP	two-ray MP

B. SIMULATION CONFIGURATION

To investigate a realistic case study, it is crucial for a PNT receiver to receive signals that possess power levels and Doppler profiles aligned with those of the reference LEO constellation. To accomplish this, a constellation propagator tool (AGI STK) was employed to simulate the LEO satellites and model the communication channels. By selecting a specific user location on Earth, the corresponding C/N_0 values experienced by the receiver during the satellite passage were extracted. Additionally, the frequency shift caused by the Doppler effect at the user's location was also collected. Utilizing the obtained C/N_0 values and Doppler profile, a binary signal generator was used to generate two signals that align with the given Doppler profile and C/N_0 level. These signals were subsequently combined within the multichannel

tracking stage of a software receiver. An overview of the simulation blocks can be seen in Fig. 7.

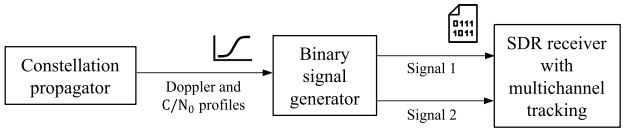


FIGURE 7. Simulation blocks. From [54].

Table 3 provides an overview of the parameter configurations employed during the test campaigns. It outlines the common settings utilized for each test. The values within the "orbital parameters","transmitter parameters", "atmospheric impairments", and "user conditions" domains were utilized to model the LEO "constellation simulator" block depicted in Fig. 7. The values specified in the "signal generator" domain were used to configure the signal simulator for generating binary samples. The values pertaining to the "receiver configuration" were set to appropriately fine-tune the software receiver for processing the generated digital signals. Additionally, Fig. 8 displays a snapshot of the simulated scenario within the LEO constellation propagator software. In this representation, the satellite is positioned directly overhead (at the zenith) in relation to the user.

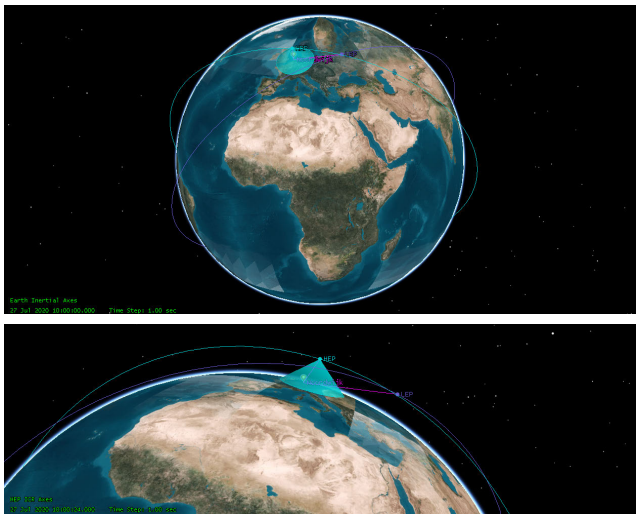


FIGURE 8. Simulated scenario showing HEP and LEP satellite passages. The transmission beamwidth cone is displayed when in LOS with the user terminal.

The simulated constellation has an orbital height of 600 km. It is among the lowest orbital heights of current and envisioned internet broadband constellations [66], [68]. It has been chosen to analyze the performance under the worst Doppler conditions of this scenario. The minimum usable elevation has been set to 28°. At the chosen orbital height, it corresponds to a transmission beamwidth of 53.5°. A reference value has been taken from Amazon's project Kuiper technical documents [66]. In these application documents, a half-cone transmission beamwidth of 48.2° is reported for the first-to-be-deployed orbital shell, which is at a 630 km height. At an orbital height of 600 km this beamwidth would result in a minimum usable elevation of about 35°. A minimum usable elevation of 28° has been assumed as a conservative choice. The assumed effective isotropic radiated power (EIRP) is 20 dBW which is the lowest value reported in Kuiper's documentation. This value is assumed in this investigation phase as a worst case.

TABLE 3. Common configuration for the experiments.

Domain	Parameter	Value
Orbital Parameters	Inclination	51.9°
	Altitude	600 km
Transmitter parameters	Modulation	BPSK(1)
	DSSS code length	1023
	Data rate	50 bit/s
	CDMA spread	20460 chips/bit
	Bandwidth	2.046 MHz
	Min. usable elevation	28°
	EIRP	20 dBW
Atmospheric impairments	Cloud and Fog model	ITU-R P840-6
	Tropospheric scintillation	ITU-R P618-12
	Ionospheric fading	ITU-R P531-13
User conditions	User location	Noordwijk (52.24°,4.45°)
Signal generator	Sampling frequency	25 MHz
	IF	0 Hz
	Code delay	0.5 ms
	Binary signal type	int8
	Quantization bits	7
	Antenna gain	3 dB
Receiver configuration	PLL order	3
	DLL order	1
	SC E-L spacing	1 chip
	MC E-L spacing	0.025 chip
	PLI threshold	0.8
	Virtual freq. separation (f_m)	18.414 MHz
	Coherent int. time	2 ms

The signals utilized in the simulations are BPSK(1) signals, possessing identical modulation characteristics to the Global Positioning System (GPS) C/A signal. The decision to employ fundamental PNT signals is in line with recent trends [55], [69], [70] and also driven by the aim of avoiding unnecessary complexity in the receiver implementation. This approach allowed us to focus on the feasibility of the proposed technique in its most basic form.

Table 4 presents the characteristics of the four Doppler scenarios, including the average C/N_0 and received power values utilized to configure the binary signal generator block (refer to Fig. 7).

TABLE 4. Scenario characterization.

Freq. band	Satellite passage	Average C/N_0 (dB-Hz)	Average power[a] (dBW)	Passage duration (s)
L	LEP	73.3	-134.1	89
L	HEP	76.3	-131.1	280
K_u	LEP	47.8	-159.6	89
K_u	HEP	51.5	-155.9	280

[a]Carrier isotropic power.

C. FIGURES OF MERIT

The primary performance metric used in the evaluation is the *code estimation error*, which is measured at the output of the DLL discriminator within the receiver's tracking stage (see Fig. 4 for the MC case). This metric, is the absolute value of the discriminator output, measured in meters.

In this analysis, we want to evaluate the performance improvement provided by the MC architecture with respect to the plain SC tracking and to compare such performance among the investigated scenarios. We leveraged the continuous code tracking results obtained throughout the observation windows to build an aggregated statistics of the signal tracking performances. Observations of the code estimation error are performed under steady-state conditions facilitated by the two-step approach, which allows for a comparison between the output of a plain SC tracking stage (first step) and the output of MC processing (second step, as shown in Fig. 3). To this purpose, the duration of SC processing was intentionally extended for a specific period, thereby ensuring sufficient data for the statistical characterization of the discriminator output. Additionally, an initial transient period was removed from the observation set to prevent any adverse effects on the accuracy of the observations. To enable a statistical comparison among the experiments, the empirical cumulative distribution function (CDF) of the code estimation errors is evaluated. The performance improvement at three different percentiles (50-th, 75-th, and 90-th) is highlighted, assessing—for each investigated scenario—the code estimation error reduction achieved by MC tracking against a conventional SC estimation.

As explained in Section II, the proposed technique introduces peak ambiguity in the ACF. This ambiguity has the potential to lead to false locking of the tracking loop, particularly for signals affected by MP impairments, and must be therefore monitored. In addition to the primary performance metric, which is the code estimation error, an additional metric of interest is the rate of change of the code estimated at the discriminator, which can be obtained from the output of the loop filter in Fig. 4. This estimated code rate can be compared with the code rate observed on a *quasi-noiseless signal*, i.e. a LOS signal with very high C/N_0 (100 dB-Hz), which is instead processed using a plain SC receiver. This comparison allows to monitor any potential biases that may arise in MP conditions due to false locking. The two code rate estimation would, in fact, differ because of noise and impairments, but on average their difference tends to zero if the MC estimation is unbiased. This average code rate error was continuously monitored across all experiments, consistently affirming the unbiased estimation capabilities of the proposed architecture even under the challenging conditions under test, thereby clearing the risk of false locking. Despite being adequate for the current validation phase of the technique, this false-lock monitoring method relies on a ground truth reference (i.e. the quasi-noiseless signal), which is typically unavailable. A practical implementation would need to rely on established methodologies detailed in literature sources [59], [63] and their incorporation into the architecture is planned for a subsequent implementation phase.

IV. RESULTS

In this section, we present the results from the simulation experiments, obtained according to the tested scenarios defined in Section III. A comprehensive discussion on the investigation outcomes under the different conditions defined by Table 2 is provided. The following discussion is organized with respect to the intensity of the Doppler phenomena in the considered LEO PNT framework, from mild (tests LS1, MP1) to moderate (tests LS2, LS3, MP2, MP3) to severe (tests LS4, MP4) conditions, depending on the combination of transmission band and satellite passage.

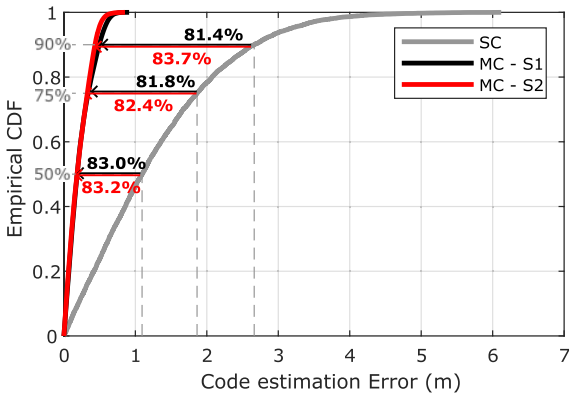
A. MILD DOPPLER CONDITIONS

The Doppler shifts experienced by the signals under the configuration of test LS1 are reported in Fig. 6a. A small divergence in the Doppler shift evolution is visible due to the 10 MHz frequency separation between f_1 and f_2. However, by looking at the empirical CDF reported in Fig. 9a, it can be observed that this received frequency difference has a small impact on the performance. The signal combination S2 is the combined processing of two received signals at respectively f_1 and f_2, but its performance is not degraded with respect to S1. This means that such a frequency separation between the channels (and the different Doppler shift experienced) is not harmful under the considered conditions. The S2 combination is behaving better, proving that under such mild Doppler conditions a small frequency separation is not challenging for the proposed architecture. Nonetheless, S1 performs similarly, despite the reduced bandwidth occupation of the transmitted channels. Both configurations yield a reduction of the code estimation error with respect to SC processing that is above 80% for all the evaluated percentiles.

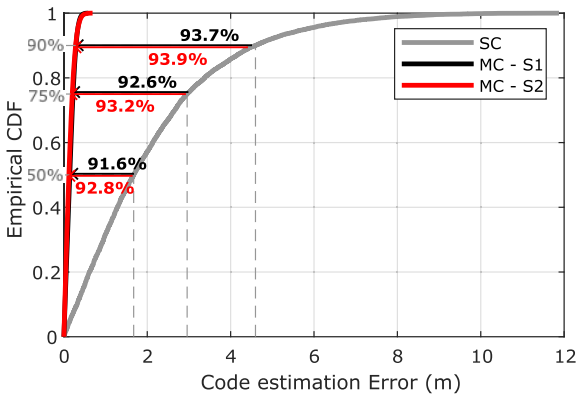
In tests MP1, MP2, MP3, and MP4 we examined the behavior of the proposed technique under MP conditions, whose characteristics are reported in Table 1. A reflected path delayed by 0.5 chip affects the SC processing by distorting the DLL discriminator function [40]. The VWB technique is based on a sharpened ACF peak, which should behave better when dealing with close-by multipath, because the contribution of the reflected path will likely fall outside a narrower main peak. It is expected that a RS such as the one defined in Table 1 will be less harmful for the MC tracking stage than for a SC stage.

During test MP1, the discriminator output observed throughout the SC phase resulted in a generally degraded code estimation error with respect to the analogous experiment in LOS conditions (test LS1). This can be inferred by comparing the upper and lower plot of Fig. 9 which highlight an obvious worsening of the SC tracking performance when a reflected path is added to the LOS signal. An MC architecture in this case can provide a great benefit thanks to the robustness to the multipath effect. The code estimation error

reduction of test LS1 is in fact improved in test MP1. In these conditions, the VWB architecture is confirmed as an effective method to limit the multipath impact.



(a) Test LS1 (LOS, L band, LEP).



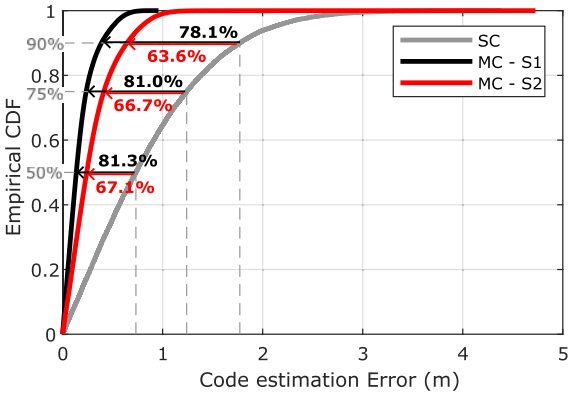
(b) Test MP1 (MP, L band, LEP).

FIGURE 9. Empirical CDF computed over code estimation errors under mild Doppler conditions. Error reduction from SC to MC is shown for three percentiles.

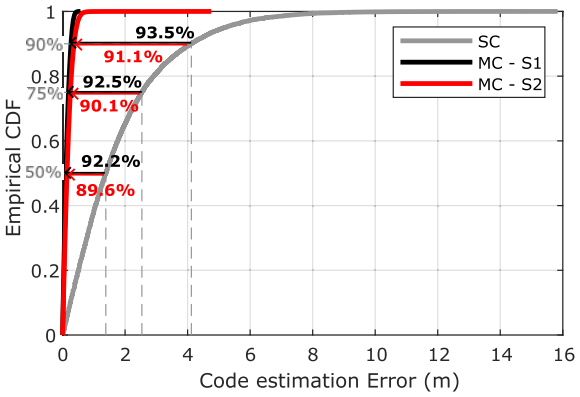
B. MODERATE DOPPLER CONDITIONS

In test LS2 we can observe the effect of a satellite passage which crosses a point that is very close to the zenith (HEP). The relative movement of the satellite with respect to the Earth-based user causes a Doppler shift in the received frequency, which is both high at low elevations and fast changing when crossing the zenith. This effect is illustrated by Fig. 6b.

The resulting empirical CDF of the code estimation error is reported in Fig 10a. This test brings in a challenging condition for signal S2. When the MC is activated for the S2 signals combination, the receiver must jointly track two channels with different carrier frequencies. But since in this case the Doppler conditions are generally more challenging than the LEP passage case, the MC stage faces a more difficult channel combination. A measure of this difficultness is provided by the code estimation error reductions for S2 shown in Fig. 10a, which is lower with respect to S1. An opposite trend with respect to what obtained in test LS1 (Fig. 9a), where a generally milder Doppler effect had a limited impact on the joint processing of two frequency-separated channels.



(a) Test LS2 (LOS, L band, HEP).



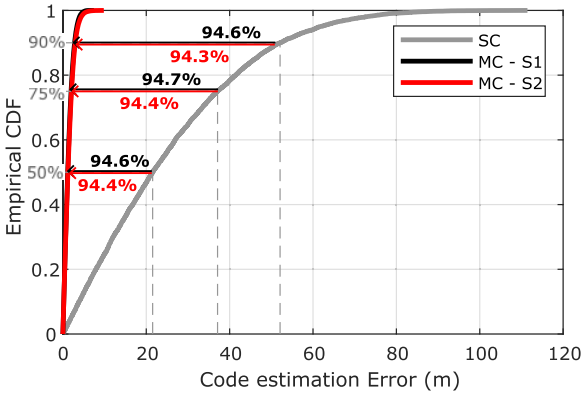
(b) Test MP2 (MP, L band, HEP).

FIGURE 10. Empirical CDF computed over code estimation errors under moderate Doppler conditions.

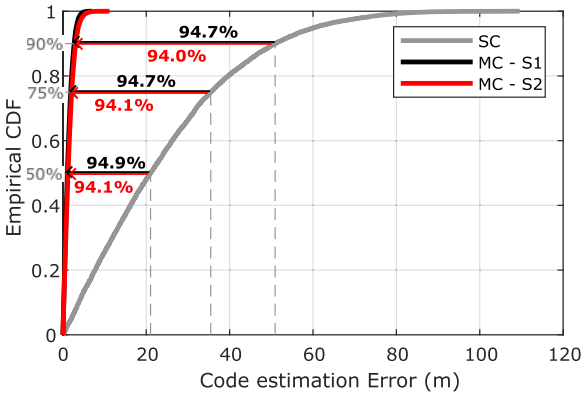
Concerning MP propagation, test MP2 involves harsher Doppler conditions with respect to test MP1, but a higher average C/N_0 level. The reported results confirm the findings of previous experiments. The two-ray multipath is again well-tolerated. The performance gain is highlighted in Fig. 10b. These capabilities are confirmed by the percentiles reductions, which are larger than those experienced in the analogous test with LOS signals (see test LS2 in Fig. 10a), for both S1 and S2. However, analogously to test LS2, the S2 signal configuration is more sensitive to the higher Doppler levels. It suffers from a lower CDF reduction with respect to S1, which should be preferred for L band signals when the relative satellite's movement is consistent with a HEP passage.

Signals in the K_u band put the proposed architecture to the test more than signals in the L band. K_u band signals are generally weaker when received on Earth (see Table 4) due to the unfavorable atmospheric absorption. Moreover, they are subject to a stronger Doppler shift due to their high position in the radio-frequency spectrum. For a LEP passage, the Doppler shift experienced by a signal transmitted in the K_u band (Fig. 6c) or in the L band (Fig. 6a) exhibits the same

trend, but far more higher Doppler shift levels. This condition provokes the large code estimation error values that are observable in Fig 11 for the SC processing mode. However, it is worth noting that in such a degraded estimation condition, the MC technique is really advantageous, providing a CDF reduction of the evaluated percentiles which is above 94% for both signal configurations of test LS3 (see Fig. 11a). This happens because the MC stage well copes with the low C/N_0 simulated in this test, improving the discriminator estimation even in presence of the fast-changing carrier frequency experienced in the K_u band. When the MC phase is triggered, the discriminator output is comparable to the SC processing performance obtained at L band. For instance, test LS1 and test LS3 were performed observing the same satellite passage. Comparing the MC outcome of test LS3 in Fig. 11a with the empirical CDF obtained for the SC stage in test LS1 (Fig. 9a) highlights the benefits of this technique when dealing with signals that are about 25 dB weaker. Moreover, the signals analyzed in test LS3 experience a Doppler shift which is, at the lowest elevations of the satellite passage, 20 times stronger than the Doppler shift of test LS1.



(a) Test LS3 (LOS, K_u band, LEP).



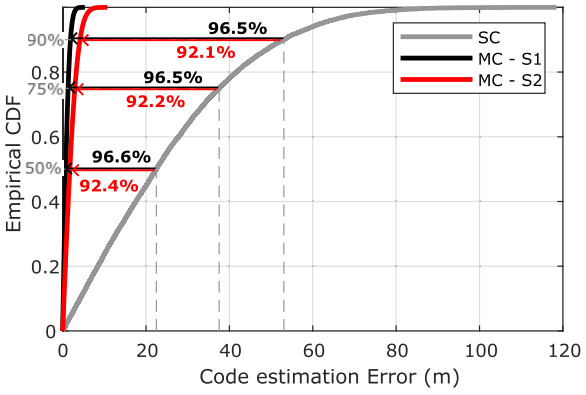
(b) Test MP3 (MP, K_u band, LEP).

FIGURE 11. Empirical CDF computed over code estimation errors under moderate Doppler conditions.

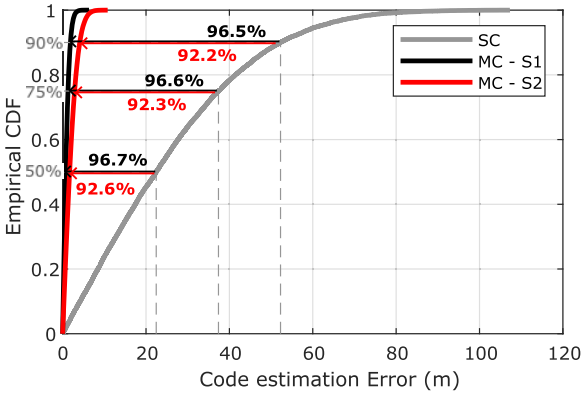
Focusing on test MP3, the empirical CDFs for the MC stage reported in Fig 11b are quite close to the MC stage values for test LS3 (Fig. 11a), obtained in the absence of multipath. The employment of a MC approach benefits the discriminator output even under low C/N_0 conditions. The result is a CDF that is again comparable with the one experienced using SC processing in test MP1, i.e. under the same multipath and satellite passage conditions, but with a C/N_0 which is about 25 dB higher (see Fig 9b).

C. SEVERE DOPPLER CONDITIONS

Analyzing the HEP passage case for the K_u band (test LS4), the findings of the previous tests are confirmed. The MC tracking is in fact capable to provide great benefits in such stressing conditions, but the high Doppler experienced for a HEP passage (Fig. 6d) challenges the S2 configuration. However, as shown in Fig. 12a, a CDF reduction above 90% characterize both S1 and S2 of test LS4 even under the strong Doppler shifts of this scenario. Nonetheless, being the Doppler conditions more intense with respect to the LEP, the processing of S2 is less advantageous than S1 due to its inherent frequency diversity that is stressed by the high Doppler. Its code estimation error reduction is in fact generally lower also with respect to what observed during test LS3 (Fig 11a), where less severe Doppler conditions were in place.



(a) Test LS4 (LOS, K_u band, HEP).



(b) Test MP4 (MP, K_u band, HEP).

FIGURE 12. Empirical CDF computed over code estimation errors under severe Doppler conditions.

Previous tests have proven the VWB technique beneficial for the code estimation error, under low C/N_0, high Doppler and using MP-affected signals. Not surprisingly, in test MP4 the S1 signal provides one of the largest empirical CDF reductions among the tests performed for this parametric analysis, as shown in Fig. 12b. A similar performance gain has been obtained in the case of test LS4, which is performed under the same conditions, but in the absence of MP (Fig. 12a). However, as also found in test LS4, the S2 signal combination is penalized by the challenging Doppler conditions caused by a HEP profile and signals transmission in the K_u band. Indeed the results reported for test MP4 in Fig 12b with S2 configuration show a an empirical CDF reduction which is slightly lower than the reduction experienced in test MP3 (Fig. 11b), under lighter Doppler shift. Again, the high sensitivity to Doppler shift of this signal configuration limits the achievable performance improvement.

Test MP3 and test MP4 were carried out under the most challenging conditions among the tests done in this parametric analysis. The presence of a RS generally reduces the performance and the transmission in the K_u band brings in a high Doppler shift and a low C/N_0 level. Nevertheless, the VWB architecture effectively copes with the investigated two-ray multipath also for K_u band signals.

V. CONCLUSION

In this work a multichannel signal tracking architecture has been proposed, consolidating its theoretical aspects. This method can work on many types of PNT channel combinations, broadening the applicability of meta-signals to encompass any form of signal orthogonality, extending beyond carrier frequency separation. The technique has shown to be highly beneficial in terms of bandwidth occupancy because the S1 multichannel configuration achieves comparable performance to the S2 configurations, where channels occupy, as a whole signal, more than twice the bandwidth. This would free up a larger amount of bandwidth resources for a potential concurrent broadband service if implemented within the context of integrated communication and navigation systems. Furthermore, the applicability domain of this architecture has been comprehensively tested varying the transmission band, the channel combination strategy, the Doppler profile, and the multipath or LOS conditions, in representative LEO PNT scenarios.

From the analysis, the benefits of the proposed technique emerge clearly. In all the configurations under test, the VWB implementation resulted beneficial. The increased complexity demanded by this architecture is traded with an improved signal tracking resulting in lower code estimation errors at the discriminator output. This improvement is effective even under strong Doppler shift levels, up to 300 kHz (see tests LS4 and MP4), and under C/N_0 as small as 47.8 dB-Hz (see tests LS3 and MP3). In all the tests, the reduction in the representative code estimation error percentiles is above 64% and more than 90% in most cases. Another clear outcome from the analysis is that in a LEO PNT scenario, such as the one described by Table 4 and 2, the technique is not impaired by a two-ray multipath signal, leading to a performance that is comparable, in all the investigated scenarios, to the performance obtained in the absence of multipath.

Besides showing the improved accuracy benefits that this multichannel approach can provide, this analysis demonstrated that the architecture can cope with harsh Doppler scenarios under several different conditions. These results represent an insightful characterization of the proposed meta-signal tracking strategy in DSSS-based wireless systems, like modern GNSS and LEO PNT scenarios. The VWB architecture is therefore potentially beneficial in a wide range of applicability domains characterizing envisioned GNSS paradigms and integrated navigation and communication satellite systems, at the cost of a larger complexity on the user side.

REFERENCES

[1] European Union Agency for the Space Program, *EUSPA EO and GNSS Market Report*. Luxembourg: Publications Office of the European Union, 2022.

[2] A. Minetto, A. Nardin, and F. Dovis, "Tight integration of GNSS measurements and GNSS-based collaborative virtual ranging," in *Proc. Int. Tech. Meeting Satell. Division Inst. Navigat.*, Miami, Florida, Oct. 2018, pp. 2399–2413.

[3] A. Minetto, A. Nardin, and F. Dovis, "GNSS-only collaborative positioning among connected vehicles," in *Proc. 1st ACM MobiHoc Workshop Technol., mOdels, Protocols Cooperat. Connected Cars*. New York, NY, USA: Association for Computing Machinery, Jul. 2019, pp. 37–42, doi: 10.1145/3331054.3331552.

[4] A. Minetto, A. Nardin, and F. Dovis, "Modelling and experimental assessment of inter-personal distancing based on shared GNSS observables," *Sensors*, vol. 21, no. 8, p. 2588, Apr. 2021. [Online]. Available: https://www.mdpi.com/1424-8220/21/8/2588

[5] M. Pini, A. Minetto, A. Vesco, D. Berbecaru, L. M. C. Murillo, P. Nemry, I. De Francesca, B. Rat, and K. Callewaert, "Satellite-derived time for enhanced telecom networks synchronization: The ROOT project," in *Proc. IEEE 8th Int. Workshop Metrology Aerosp. (MetroAeroSpace)*, Jun. 2021, pp. 288–293.

[6] W. Wang, N. Okati, I. Tanash, T. Riihonen, and E.-S. Lohan, "Location-based beamforming architecture for efficient farming applications with drones," in *Proc. Int. Conf. Localization GNSS (ICL-GNSS)*, Jun. 2019, pp. 1–6.

[7] O. Vouch, A. Nardin, A. Minetto, S. Zocca, M. Valvano, and F. Dovis, "Aided Kalman filter models for GNSS-based space navigation," *IEEE J. Radio Freq. Identificat.*, vol. 8, pp. 535–546, 2024.

[8] O. Vouch, A. Nardin, A. Minetto, S. Zocca, F. Dovis, L. Konitzer, J. K. Joel Parker, B. Ashman, F. Bernardi, S. Tedesco, and S. Fantinato, "Bayesian integration for deep-space navigation with GNSS signals," in *Proc. 27th Int. Conf. Inf. Fusion (FUSION)*, Jul. 2024, pp. 1–8.

[9] A. Nardin, A. Minetto, O. Vouch, M. Mariani, and F. Dovis, "Snapshot acquisition of GNSS signals in space: A case study at lunar distances," in *Proc. Int. Tech. Meeting Satell. Division Inst. Navigat.*, Denver, CO, USA, Oct. 2022, pp. 3603–3617.

[10] A. Nardin, A. Minetto, S. Guzzi, F. Dovis, L. Konitzer, and J. J. K. Parker, "Snapshot tracking of GNSS signals in space: A case study at lunar distances," in *Proc. Int. Tech. Meeting Satell. Division Inst. Navigat.*, Denver, CO, USA, Oct. 2023, pp. 3267–3281.

[11] A. Nardin, T. Imbiriba, and P. Closas, "Jamming source localization using augmented physics-based model," in *Proc. IEEE Int. Conf. Acoust., Speech Signal Process. (ICASSP)*, Jun. 2023, pp. 1–5.

[12] A. Nardin, T. Imbiriba, and P. Closas, "Crowdsourced jammer localization using APBMs: Performance analysis considering observations disruption," in *Proc. IEEE/ION Position, Location Navigat. Symp. (PLANS)*, Apr. 2023, pp. 511–519.

[13] R. Hirokawa, I. Fernández-Hernández, and S. Reynolds, "PPP/PPP-RTK open formats: Overview, comparison, and proposal for an interoperable message," *NAVIGATION, J. Inst. Navigat.*, vol. 68, no. 4, pp. 759–778, Dec. 2021. [Online]. Available: https://navi.ion.org/content/68/4/759

[14] X. Zhang, Z. Yao, and M. Lu, "Optimizing the Gabor bandwidth of satellite navigation signals by MCS signal expression," *Sci. China Phys., Mech. Astron.*, vol. 54, no. 6, pp. 1077–1082, Jun. 2011.

[15] A. Nardin, F. Dovis, S. Perugia, C. Cristodaro, and V. Valle, "Optimised design of next-generation multiplexing schemes for global navigation satellite systems," *IET Radar, Sonar Navigat.*, vol. 17, no. 7, pp. 1100–1104, Jul. 2023, doi: 10.1049/rsn2.12403.

[16] L. Deng, Y. Yang, J. Ma, Y. Feng, L. Ye, and H. Li, "OFDM-BOC: A broadband multicarrier navigation modulation-based BOC for future GNSS," *IEEE Trans. Veh. Technol.*, vol. 73, no. 3, pp. 3964–3979, Mar. 2024.

[17] A. Emmanuele, M. Luise, F. Zanier, and M. Crisci, "Selective accuracy and multiresolution capabilities are intrinsic features of multicarrier waveforms for GNSS," in *Proc. 6th ESA Workshop Satell. Navigat. Technol. (Navitec) Eur. Workshop GNSS Signals Signal Process.*, Dec. 2012, pp. 1–8.

[18] P. Dabove and V. Di Pietra, "Towards high accuracy GNSS real-time positioning with smartphones," *Adv. Space Res.*, vol. 63, no. 1, pp. 94–102, Jan. 2019. [Online]. Available: https://www.sciencedirect.com/science/article/pii/S0273117718306537

[19] Z. Yan, X. Chen, X. Tang, and L. Ruotsalainen, "A novel carrier loop based on adaptive LM-QN method in GNSS receivers," *IEEE Trans. Veh. Technol.*, vol. 71, no. 5, pp. 5259–5271, May 2022.

[20] P. Teunissen and O. Montenbruck, *Springer Handbook of Global Navigation Satellite Systems*. Berlin, Germany: Springer, 2017.

[21] J. Rodríguez, "On generalized signal waveforms for satellite navigation," Ph.D. dissertation, Fac. Aerosp. Eng., Univ. der Bundeswehr München, 2008.

[22] Z. Yao, J. Ma, J. Zhang, and M. Lu, "Multicarrier constant envelope composite signal—A solution to the next generation satellite navigation signals," in *Proc. Int. Tech. Meeting Satell. Division Inst. Navigat.*, Nov. 2017, pp. 1520–1533. [Online]. Available: https://www.ion.org/publications/abstract.cfm?articleID=15372

[23] Z. Yao, F. Guo, J. Ma, and M. Lu, "Orthogonality-based generalized multicarrier constant envelope multiplexing for DSSS signals," *IEEE Trans. Aerosp. Electron. Syst.*, vol. 53, no. 4, pp. 1685–1698, Aug. 2017. [Online]. Available: http://ieeexplore.ieee.org/document/7858582/

[24] R. Knight. (2022). *ESA Outlines Plans for Demo of LEO PNT Satellites As Part of FutureNAV, Gives Other Updates*. Inside GNSS. Accessed: Dec. 31, 2022. [Online]. Available: https://insidegnss.com/esa-outlines-plans-for-demo-of-leo-pnt-satellites-as-part-of-futurenav-gives-other-updates/

[25] F. S. Prol, R. M. Ferre, Z. Saleem, P. Välisuo, C. Pinell, E. S. Lohan, M. Elsanhoury, M. Elmusrati, S. Islam, K. Çelikbilek, K. Selvan, J. Yliaho, K. Rutledge, A. Ojala, L. Ferranti, J. Praks, M. Z. H. Bhuiyan, S. Kaasalainen, and H. Kuusniemi, "Position, navigation, and timing (PNT) through low Earth orbit (LEO) satellites: A survey on current status, challenges, and opportunities," *IEEE Access*, vol. 10, pp. 83971–84002, 2022.

[26] T. G. Reid, B. Chan, A. Goel, K. Gunning, B. Manning, J. Martin, A. Neish, A. Perkins, and P. Tarantino, "Satellite navigation for the age of autonomy," in *Proc. IEEE/ION Position, Location Navig. Symp. (PLANS)*, Portland, OR, USA, Apr. 2020, pp. 342–352. [Online]. Available: https://ieeexplore.ieee.org/document/9109938/

[27] F. van Diggelen, "High-sensitivity GNSS," in *Position, Navigation, and Timing Technologies in the 21st Century*. Hoboken, NJ, USA: Wiley, 2020, pp. 445–479, doi: 10.1002/9781119458449.ch18.

[28] A. Nardin, F. Dovis, and J. A. Fraire, "Empowering the tracking performance of LEO-based positioning by means of meta-signals," *IEEE J. Radio Freq. Identificat.*, vol. 5, no. 3, pp. 244–253, Sep. 2021.

[29] A. Nardin, F. Dovis, and J. A. Fraire, "Empowering the tracking performance of LEO PNT by means of meta-signals," in *Proc. IEEE Int. Conf. Wireless Space Extreme Environments (WiSEE)*, Oct. 2020, pp. 153–158.

[30] Z. Yao and M. Lu, *Next-Generation GNSS Signal Design*. Singapore: Springer, 2021.

[31] J.-L. Issler, M. Paonni, and B. Eissfeller, "Toward centimetric positioning thanks to L- and S-band GNSS and to meta-GNSS signals," in *Proc. 5th ESA Workshop Satell. Navigat. Technol. Eur. Workshop GNSS Signals Signal Process. (NAVITEC)*, Dec. 2010, pp. 1–8.

[32] M. Paonni, J. Curran, M. Bavaro, and J. Fortuny, "GNSS meta-signals: Coherently composite processing of multiple GNSS signals," in *Proc. 27th Int. Tech. Meeting The Satell. Division Inst. Navigat.*, Tampa, FL, USA, 2014, pp. 8–12.

[33] P. Das, L. Ortega, J. Vilá-Valls, F. Vincent, E. Chaumette, and L. Davain, "Performance limits of GNSS code-based precise positioning: GPS, Galileo & meta-signals," *Sensors*, vol. 20, no. 8, p. 2196, Apr. 2020. [Online]. Available: https://www.mdpi.com/1424-8220/20/8/2196

[34] L. Ortega, D. Medina, J. Vilá-Valls, F. Vincent, and E. Chaumette, "Positioning performance limits of GNSS meta-signals and HO-BOC signals," *Sensors*, vol. 20, no. 12, p. 3586, Jun. 2020. [Online]. Available: https://www.mdpi.com/1424-8220/20/12/3586

[35] D. Borio and C. Gioia, "Reconstructing GNSS meta-signal observations using sideband measurements," *NAVIGATION, J. Inst. Navigat.*, vol. 70, no. 1, 2023, Art. no. navi.558. [Online]. Available: https://navi.ion.org/content/70/1/navi.558

[36] D. Borio, "Hypercomplex representation and processing of GNSS signals," in *Proc. Int. Tech. Meeting Satell. Division Inst. Navigat.*, Oct. 2022, pp. 3160–3179.

[37] M. S. Hameed, T. Woerz, T. Pany, J. Wendel, M. Paonni, and T. Senni, "Demonstration of meta-signal positioning using LAMBDA ambiguity fixing method within a bit-true simulation," in *Proc. Int. Tech. Meeting Satell. Division Inst. Navigat.*, Oct. 2021, pp. 2819–2837.

[38] J. Garcia-Molina, "Unambiguous meta-signal processing: A path to code-based high-accuracy PNT," *Inside GNSS*, vol. 16, no. 2, pp. 50–55, Mar. 2021.

[39] C. Wang, X. Cui, T. Ma, S. Zhao, and M. Lu, "Asymmetric dual-band tracking technique for optimal joint processing of BDS B1I and B1C signals," *Sensors*, vol. 17, no. 10, p. 2360, Oct. 2017. [Online]. Available: https://www.mdpi.com/1424-8220/17/10/2360

[40] E. Kaplan and C. Hegarty, *Understanding GPS/GNSS: Principles and Applications*. Norwood, MA, USA: Artech House, 2017.

[41] W. Zhang, Z. Yao, and M. Lu, "WHAT: Wideband high-accuracy joint tracking technique for BDS B1 composite signal," in *Proc. IEEE 9th Int. Conf. Electron. Inf. Emergency Commun. (ICEIEC)*, Jul. 2019, pp. 178–182.

[42] Y. Gao, Z. Yao, and M. Lu, "High-precision unambiguous tracking technique for BDS B1 wideband composite signal," *NAVIGATION*, vol. 67, no. 3, pp. 633–650, Sep. 2020, doi: 10.1002/navi.377.

[43] Z. Tian, X. Cui, G. Liu, and M. Lu, "LPRA-DBT: Low-processing-rate asymmetrical dual-band tracking method for BDS-3 B1I and B1C composite signal," in *Proc. Int. Tech. Meeting The Inst. Navigat.*, Feb. 2022, pp. 1027–1038.

[44] C. Schwalm, C. Enneking, and S. Thoelert, "Ziv-zakai bound and multicorrelator compression for a Galileo E1 meta-signal," in *Proc. Eur. Navigat. Conf. (ENC)*, Nov. 2020, pp. 1–9.

[45] European Union. (Jan. 2021). *European GNSS (Galileo) Open Service, Signal-in-Space Interface Control Document (OS SIS ICD V2.0)*. [Online]. Available: https://www.gsc-europa.eu/sites/default/files/sites/all/files/GalileoOSSISICDv2.0.pdf

[46] T. Reid, "Opportunities in commercial LEO satellite navigation," in *Proc. Int. Tech. Meeting Satell. Division Inst. Navigat.*, Oct. 2021, pp. 2012–2048. [Online]. Available: http://www.ion.org/publications/abstract.cfm?jp=p&articleID=18106

[47] P. A. Iannucci and T. E. Humphreys, "Economical fused LEO GNSS," in *Proc. IEEE/ION Position, Location Navigat. Symp. (PLANS)*, Apr. 2020, pp. 426–443.

[48] G. Gutt, D. Lawrence, S. Cobb, and M. O'Connor, "Recent PNT improvements and test results based on low Earth orbit satellites," in *Proc. Int. Tech. Meeting The Inst. Navigat.*, Feb. 2018, pp. 570–577.

[49] T. G. R. Reid, A. M. Neish, T. Walter, and P. K. Enge, "Broadband LEO constellations for navigation," *Navigation*, vol. 65, no. 2, pp. 205–220, Jun. 2018. [Online]. Available: https://onlinelibrary.wiley.com/doi/abs/10.1002/navi.234

[50] S. Hayek, J. Saroufim, M. Neinavaie, S. Kozhaya, and Z. M. Kassas, "Assessment of differential Doppler navigation with starlink LEO satellite signals of opportunity," in *Proc. Int. Tech. Meeting The Inst. Navigat.*, Feb. 2023, pp. 1021–1031.

[51] J. Khalife and Z. M. Kassas, "Performance-driven design of carrier phase differential navigation frameworks with megaconstellation LEO satellites," *IEEE Trans. Aerosp. Electron. Syst.*, vol. 59, no. 3, pp. 2947–2966, Jun. 2023.

[52] J. Zhu, Y. Sun, and M. Peng, "Timing advance estimation in low Earth orbit satellite networks," *IEEE Trans. Veh. Technol.*, vol. 73, no. 3, pp. 4366–4382, Mar. 2024.
[53] A. Nardin, F. Dovis, and B. Motella, "Impact of non-idealities on GNSS meta-signals processing," in *Proc. Eur. Navigat. Conf. (ENC)*, Dresden, Germany, Nov. 2020, pp. 1–8.
[54] A. Nardin, F. Dovis, F. Zanier, and F. Melman, "Flexible metasignal tracking: Architecture robustness in challenging PNT scenarios," *IEEE Trans. Aerosp. Electron. Syst.*, vol. 60, no. 3, pp. 3095–3107, Jun. 2024.
[55] L. Ries, M. C. Limon, F.-C. Grec, M. Anghileri, R. Prieto-Cerdeira, F. Abel, J. Miguez, J. V. Perello-Gisbert, S. D'Addio, R. Ioannidis, A. Ostillio, M. Rapisarda, R. Sarnadas, and P. Testani, "LEO-PNT for augmenting Europe's space-based PNT capabilities," in *Proc. IEEE/ION Position, Location Navigat. Symp. (PLANS)*, Apr. 2023, pp. 329–337.
[56] R. McDonough and A. Whalen, *Detection of Signals in Noise*. Amsterdam, The Netherlands: Elsevier, 1995, pp. 383–445.
[57] J. W. Betz and K. R. Kolodziejski, "Generalized theory of code tracking with an early-late discriminator, Part I: Lower bound and coherent processing," *IEEE Trans. Aerosp. Electron. Syst.*, vol. 45, no. 4, pp. 1538–1556, Oct. 2009. [Online]. Available: https://ieeexplore.ieee.org/document/5310316/
[58] J. W. Betz, "The offset carrier modulation for GPS modernization," in *Proc. Nat. Tech. Meeting The Inst. Navigat.*, San Diego, CA, USA, 1999, pp. 639–648.
[59] A. Nardin, "Innovative signal processing solutions for next-generation satellite navigation systems," Ph.D. dissertation, Dept. Electron. Telecommun., Politecnico di Torino, 2023.
[60] B. MacLennan, "Gabor representations of spatiotemporal visual images," Dept. Comput. Sci., Univ. Tennessee, Knoxville, TN, USA, Tech. Rep. CS-91-144, 1991.
[61] A. Weiss and E. Weinstein, "Fundamental limitations in passive time delay estimation—Part I: Narrow-band systems," *IEEE Trans. Acoust., Speech, Signal Process.*, vol. ASSP-31, no. 2, pp. 472–486, Apr. 1983.
[62] E. Weinstein and A. Weiss, "Fundamental limitations in passive time-delay estimation—Part II: Wide-band systems," *IEEE Trans. Acoust., Speech, Signal Process.*, vol. ASSP-32, no. 5, pp. 1064–1078, Oct. 1984.
[63] J. Wendel, F. M. Schubert, and S. Hager, "A robust technique for unambiguous BOC tracking," *Navigation*, vol. 61, no. 3, pp. 179–190, Sep. 2014.
[64] Z. Yao, Y. Gao, Y. Gao, and M. Lu, "Generalized theory of BOC signal unambiguous tracking with two-dimensional loops," *IEEE Trans. Aerosp. Electron. Syst.*, vol. 53, no. 6, pp. 3056–3069, Dec. 2017.
[65] J. J. Spilker Jr., P. Axelrad, B. W. Parkinson, and P. Enge, *Global Positioning System: Theory and Applications, Volume I*. Washington, DC, USA: American Institute of Aeronautics and Astronautics, Inc., 1996.
[66] *Application of Kuiper Systems LLC for Authority to Launch and Operate a Non-Geostationary Satellite Orbit System in Ka-Band Frequencies and Attachments*, Amazon, Seattle, WA, USA, 2019.
[67] S. D. Bast, J.-M. Sleewaegen, and W. D. Wilde, "Analysis of multipath code-range errors in future LEO-PNT systems," *Eng. Proc.*, vol. 54, no. 1, p. 34, Oct. 2023. [Online]. Available: https://www.mdpi.com/2673-4591/54/1/34
[68] M. Su, X. Su, Q. Zhao, and J. Liu, "BeiDou augmented navigation from low Earth orbit satellites," *Sensors*, vol. 19, no. 1, p. 198, Jan. 2019. [Online]. Available: https://www.mdpi.com/1424-8220/19/1/198
[69] N. S. Miller, J. T. Koza, S. C. Morgan, S. M. Martin, A. Neish, R. Grayson, and T. Reid, "SNAP: A xona space systems and GPS software-defined receiver," in *Proc. IEEE/ION Position, Location Navigat. Symp. (PLANS)*, Apr. 2023, pp. 897–904.
[70] W. Li, Q. Yang, X. Du, M. Li, Q. Zhao, L. Yang, Y. Qin, C. Chang, Y. Wang, and G. Qin, "LEO augmented precise point positioning using real observations from two CENTISPACE^{TM} experimental satellites," *GPS Solutions*, vol. 28, no. 1, pp. 1–13, Dec. 2023, doi: 10.1007/s10291-023-01589-0.



ANDREA NARDIN (Member, IEEE) received the M.Sc. degree in telecommunications engineering and the Ph.D. degree (Hons.) in electrical, electronics and communications engineering from the Politecnico di Torino, Turin, Italy, in 2018 and 2023, respectively. Since 2018, he has been with the Navigation Signal Analysis and Simulation (NavSAS) Group, Politecnico di Torino. In 2021, he was a Visiting Doctoral Researcher with the Information Processing Laboratory (IPL), Northeastern University, Boston, MA, USA. He is currently an Assistant Professor with the Department of Electronics and Telecommunications, Politecnico di Torino. His research interests include signal processing architectures and signal design applied to GNSSs and next-generation PNT systems.



FABIO DOVIS (Member, IEEE) was born in Bruino, Italy, in 1970. He received the M.Sc. and Ph.D. degrees from the Politecnico di Torino, Turin, Italy, in 1996 and 2000, respectively. He joined the Department of Electronics and Telecommunications, Politecnico di Torino, as an Assistant Professor, in 2004, and as an Associate Professor, in 2014. Since 2021, he has been a Full Professor with the Department of Electronics and Telecommunications, where he coordinates the Navigation Signal Analysis and Simulation (NavSAS) Research Group. He has a relevant experience in European projects in satellite navigation and cooperation with industries and research institutions. His research interests include the design of GPS and Galileo receivers and advanced signal processing for interference and multipath detection and mitigation and ionospheric monitoring. He serves as a member for the IEEE Aerospace and Electronics Systems Society Navigation Systems Panel.



FRANCESCA ZANIER received the M.Sc. degree in telecommunications engineering and the Ph.D. degree from the University of Pisa, Italy. She joined European Space Agency, ESTEC, Noordwijk, The Netherlands, in 2009, where she is currently a Radio Navigation System Engineer with the Radio Navigation Systems and Techniques Section of the Technical Directorate. Her research interests include signal processing, estimation theory, GNSS receivers, and signals and navigation applications.



FLOOR MELMAN received the master's degree in aerospace engineering from Delft University of Technology (TU Delft), in 2018. From December 2018 to August 2020, he was a Young Graduate Trainee (YGT) in the Navigation Directorate on Galileo signals and receivers. Since 2020, he has been a Radio Navigation Engineer with ESA/ESTEC. His main areas of work include PNT algorithms (in harsh environments) and GNSS signal processing.